Computers in Biology and Medicine 42 (2012) 387–393

Contents lists available at SciVerse ScienceDirect

Computers in Biology and Medicine

journal homepage: www.elsevier.com/locate/cbm

Artifacts in wearable photoplethysmographs during daily life motions and their reduction with least mean square based active noise cancellation method

Hyonyoung Han [1], Jung Kim *

Department of Mechanical Engineering, KAIST, 373-1, Guseong-Dong, Yuseong-Gu, Daejeon, 305-701, Republic of Korea

ARTICLE INFO

Article history:
Received 20 January 2011
Received in revised form
10 August 2011
Accepted 5 December 2011

Keywords:
Photoplethysmograph
Daily life motion
Motion artifact
Artifact reduction
Active noise cancellation

ABSTRACT

Signal distortion of photoplethysmographs (PPGs) due to motion artifacts has been a limitation for developing real-time, wearable health monitoring devices. The artifacts in PPG signals are analyzed by comparing the frequency of the PPG with a reference pulse and daily life motions, including typing, writing, tapping, gesturing, walking, and running. Periodical motions in the range of pulse frequency, such as walking and running, cause motion artifacts. To reduce these artifacts in real-time devices, a least mean square based active noise cancellation method is applied to the accelerometer data. Experiments show that the proposed method recovers pulse from PPGs efficiently.

1. Introduction

Photoplethysmographs (PPGs) are a popular, noninvasive health monitoring device for measuring the heart rate, blood oxygen saturation, blood pressure, cardiac output, and respiration [1]. Although PPGs have been used in clinical applications, accurate and reliable measurements of heart rate are achieved only while the subject maintains a stationary posture. It is difficult to obtain the PPG signal without artifacts during certain motions, and this difficulty limits the application of wearable devices. The reduction of motion artifacts is especially difficult because their major frequency components overlap with those of the PPG signal.

Because common filter methods with a fixed cutoff frequency are unsuccessful in reducing motion artifacts, researchers in the last decade have proposed two methods to reduce motion artifacts. The first is a non-motion reference method that extracts the pulse signal from the distorted PPG signal based on the supposition that the pulse signal is a major component in the measured signal and that its frequency slowly changes in contrast to the artifacts [2–7]. This method is unsuitable for wearable devices because it is time consuming and requires a large amount of data and a high sampling frequency for the extraction of the PPG signal. The second category is a motion reference method that uses reference body motion sensors [8–10]. The method uses active noise cancellation and requires a filter optimization algorithm. The laguerre [9], least mean square (LMS) [10], recursive least square (RLS) [11,12], principle component analysis (PCA) [13], and Widrow–Hoff learning rule [14] are proposed as optimization algorithms for simple motions, such as horizontal and vertical hand waving and finger bending and pressing. However, because daily life motions are more complex, these algorithms are unsuitable.

The characteristics of the artifacts arising from daily life motions in the PPG signal must be studied analytically to gain a better understanding of the motion artifacts' spectral distributions [15–17], movement range, and periodicity. Motions in daily life that affect the measurement of the PPG on the finger can be classified according to the location of the joint: finger motions according to finger joints and arm motions according to shoulder and elbow joints. Finger motions cover a small movement range. Object exploration and texture scanning involve small, slow, non-periodic motions in the 0.8–2.2 Hz range. Handwriting and typing are similar to exploration and scanning but have higher frequencies (4.0–7.0 Hz). Tapping involves small, fast, and comparatively periodic finger motions. The arm motions are generally large and periodic. Gesturing, which includes unconscious motion while speaking, consists of broad and comparatively non-periodic motions (0.0–4.0 Hz). Running is a broad, fast, and distinct

* Corresponding author. Tel.: +82 42 350 3231; fax: +82 42 350 5230.
E-mail addresses: hhn98@kaist.ac.kr (H. Han), jungkim@kaist.ac.kr (J. Kim).
[1] Tel.: +82 42 350 3271; fax: +82 42 350 5230.

0010-4825/$ - see front matter © 2011 Elsevier Ltd. All rights reserved.
doi:10.1016/j.compbiomed.2011.12.005

periodic motion (2.0–3.0 Hz); walking is similar to, though slower than, running. Therefore, the frequency components of running and walking are crowded narrowly in one dominant frequency, whereas gesturing has a wide frequency band. This work analyzes these motions, specifically their three-directional components in a corrupted PPG signal. The results are discussed in terms of the artifact properties that affect the PPG for each motion.

This work presents an artifact reduction method with a wearable PPG for six representative daily life motions. The artifact properties of the PPG signal during the motions are analyzed, and the distortion effects on the artifacts are verified. In Section 2, the wearable device and the artifact reduction algorithms are described with simple backgrounds. Section 3 describes the analysis of the motion artifacts and their reduction.

2. Methods

2.1. Photoplethysmograph

The PPG uses a light source and a photo detector to observe volume changes in blood vessels within tissues [18]. When light is emitted onto the tissue, some of the light is reflected, some absorbed, and some transmitted. The detected signal contains two main components: quasi-DC and AC. The quasi-DC component consists of static signals reflected from the static elements of body tissue, such as the epidermis, dermis, hypodermis, and bone; it also includes the barely changing signals from respiration, vasomotor activity, and vasoconstrictor waves [18–20]. The AC component is a dynamically changing signal that arises from changes in the signal reflected from the blood vessels; the morphology of the blood vessels change due to the pulse. The changes in the morphology affect the reflective rate coefficient of the optical property of the vessels. The heart rate is computed by counting the pulses from the obtained waveforms. Because the frequency of the human heart rate generally ranges from 0.8 to 2 Hz [1], this particular range of the measured pulse is of interest here.

2.2. Active noise cancellation

As shown in Fig. 1, an active noise cancellation algorithm obtains the desired signal by subtracting the estimated undesired noise [21]. Our desired signal is pulse, $S(n)$, but what is obtained from the PPG is a measurement signal, $D(n)$, which is expressed as a combination of the $S(n)$ and the undesired motion artifacts, $N(n)$:

$$D(n) = S(n) + N(n) \tag{1}$$

The $N(n)$ is hard to measure directly; the $N(n)$ is estimated from measurable motion data, $X(n)$ because both $N(n)$ and $X(n)$ have the same source, motion. Hence, the estimated pulse, $S'(n)$, can be extracted by subtracting the estimated motion artifacts from the $D(n)$ as follows:

$$e(n) = S'(n) = D(n) - N'(n) \tag{2}$$

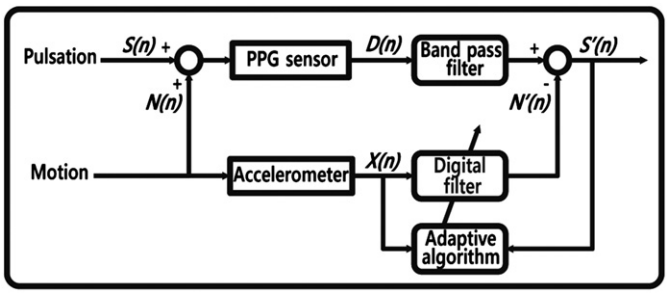

Fig. 1. Block diagram of an active noise cancellation algorithm.

The $X(n)$ is converted to the estimated motion artifacts, $N'(n)$, using an adaptive filter. The adaptive filter consists of two parts: an adaptive algorithm and a digital filter. General digital filters are used for a fixed bandwidth, but an adaptive filter can change the filter bandwidth by changing its coefficient on the basis of the input, the environment, and the output characteristics. Using this continuously changing filter coefficient, $w(n)$, the estimated artifacts, $N'(n)$, can be determined by filtering $X(n)$ using the following equation:

$$N'(n) = w(n) \times X(n) \tag{3}$$

The function of the adaptive algorithm is to determine the proper filter coefficient for extracting motion information, $N'(n)$, from $X(n)$. The least mean square method is used to update the filter coefficient. The method has a high level of stability and a low filter order [22]. Filter coefficients are updated and calculated instantaneously to minimize the derivative, $d\xi(n)/dn$ of the root mean square error, $\xi(n)$. These processes, which are expressed as follows, minimize the errors and optimize the filter coefficient $w(n)$:

$$\xi(n) = \sqrt{e^2(n)} \tag{4}$$

$$\frac{d\xi(n)}{dn} = \frac{d}{dn}\sqrt{e^2(n)} = -N(n) \times e(n) \tag{5}$$

The filter coefficient $w(n)$ can be expressed as the sum of past coefficients and the gradient of the root mean square error with step size μ, (6).

$$w(n+1) = w(n) + \mu \times \frac{d}{dn}\xi(n) \tag{6}$$

In this research, an accelerometer that is not influenced by the cardiac pulse is used as a motion sensor. The motion information is reduced from three-directional signals in rectangular coordinates to two-directional signals in cylindrical coordinates, the longitudinal and radial directions of the finger [23], by considering the shape of the blood vessel. The x-direction is aligned with the longitudinal direction of the finger. The y and z directions, which are aligned perpendicular to the longitudinal direction of the finger, are converted to the magnitude of a vector in the radial direction of the finger.

The design of the adaptive filter should be selected with regard to data consumption and operating time so that the filter order, related to the output quality, and the step size (μ) relate to the system convergence. Gibbs [8] used the 15th-order filter with 100-Hz sampling frequency, Relente [11] used the 32nd-order filter with 200-Hz sampling frequency, and Kim [4] used the 30th-order filter with 200 Hz sampling frequency. The filter orders and sampling frequencies indicate that these adaptive filters should cover higher than 0.15 s window size. In our case, a device with a sampling frequency of 20 Hz, which is sufficient to obtain the features of the pulse signal, was chosen. Therefore, a third-order adaptive filter is employed to cover the window size.

Fig. 2 shows the output signal with different step sizes from 0.01 to 0.21. At a lower step size, the high-frequency motion noise is filtered well, but a slowly changing baseline remains. On the other hand, a higher step size reduces the low-frequency components but remains too noisy. Above 0.21, the signal is too noisy; hence, it is omitted. The heart rates determined from the signals in Fig. 2 using the zero-crossing method described below are 31, 21, 17, 17, 19, 24, 24, and 24 pulses, and the count of the reference is 17 pulses for 20 s. Therefore, based on the counted heart rate, a

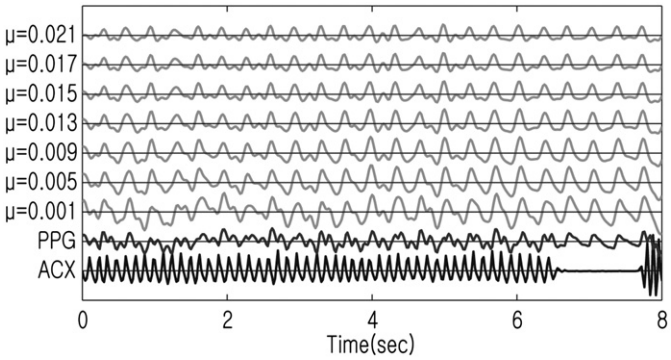

Fig. 2. Effect of the step size (μ) on the adaptive filter performance; base line (ACX) shows acceleration signal, dark gray line presents distorted PPG signal and above 7 light gray lines are reconstructed PPG signals as step size.

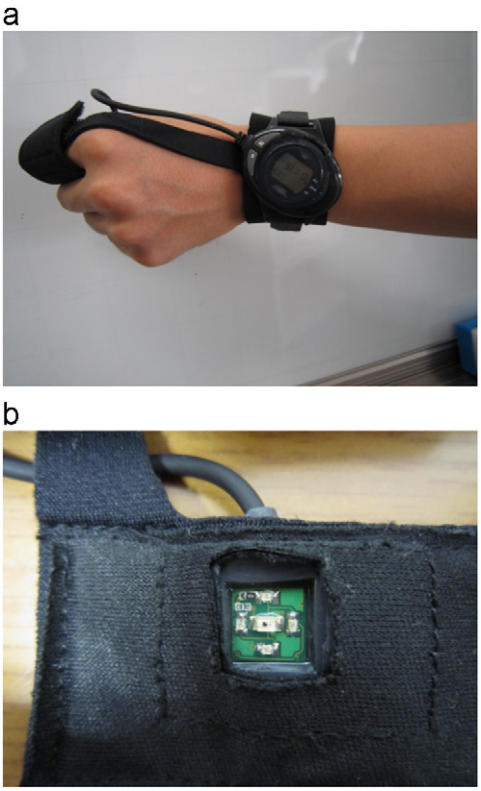

Fig. 3. (a) Glove-type wearable device; (b) four LEDs and photodiode for PPG.

step size of 0.009 that sufficiently reduces the baseline changes and the high-frequency order was used.

2.3. Wearable PPG

A glove-type wearable device was developed to measure the heart rate. The device has three main parts: a sensor, an analog circuit, and a microprocessor unit (MPU). The sensor part consists of two sensors: an optical sensor for the PPG and a three-axis accelerometer for motion. The optical sensor includes one photodiode and four infrared (IR) LEDs with 940-nm wavelengths to reduce external light, shown in Fig. 3. The accelerometer (ADXL330, Analog Devices, USA) is located on the opposite side of the optical sensor. They are positioned on the finger with an adjustable *Velcro* strap. The circuit ($55\,\text{mm} \times 42\text{mra} \times 12\text{mra}$) extracts the pulse with a reduced level of noise, requiring the gradual application of band-pass filters and amplifiers. Two passive high- and low-pass filters with cutoff frequencies of 0.3 to 5 Hz are employed, and the filtered signal is amplified with a gain of 2000. Additionally, a digital filter extracts the pulse with a narrower frequency band than the analog filter. A second-order infinite impulse response Butterworth filter is used to reduce the signal outside the range of 0.700. to 2.5to . The motion artifact reduction algorithm is then processed. The analog filter and digital signal processing produce a phase shift and a time delay compared with the recorded raw data; however, the delay consumes less than 10Tms, and the PPG heart rate is not influenced.

The low-power microprocessor (MSP430FG439, Texas Instruments, USA) handles the analog to digital convert (ADC), the digital filtering, the peak detection using a modified downward zero-crossing peak detection algorithm, and the wireless communication. The amplified and filtered PPG signals as well as the accelerometer signals are sampled at a frequency of 20 Hz with a 12-bit resolution. The sampling rate is sufficient to obtain the PPG signal because the frequency range of the PPG waveform and motion signal is less than 10 Hz. A low-power RF device (nRF24L01, Nordic, NOR) is used for wireless communication at a distance of up to 10 m and transmits two types of data: the calculated heart rate at 10-second intervals or the PPG, accelerometer, and reconstructed PPG data at the sampling time.

2.4. Experimental setup

Eleven healthy subjects (age, 30.0 ± 7.07 years) were tested to study the frequency properties of daily life motions. The KAIST Institutional Review Board approved the experimental protocol and the publication of this study. The subjects were asked to perform six motions: typing, writing, tapping, gesturing, walking, and running. During the experiment, they were asked to move both hands naturally without any consciousness. The data from typing, writing, tapping, and gesturing were measured for one

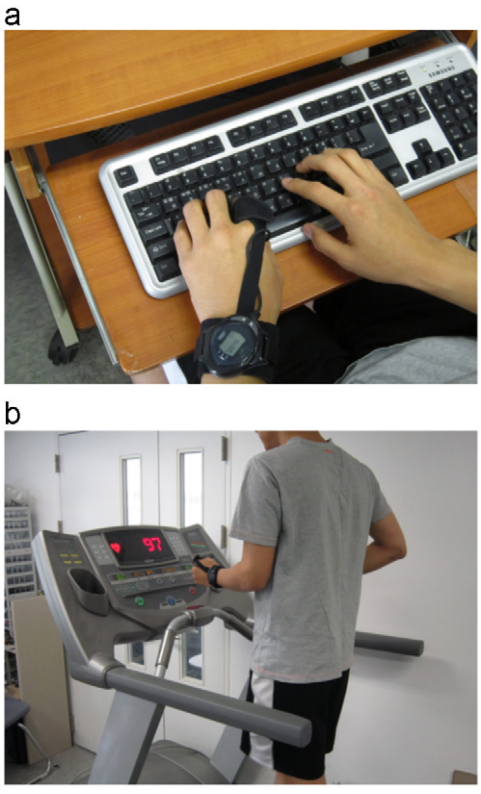

Fig. 4. Experimental setup: (a) typing and (b) running.

minute each, and the data for walking and running were measured for 5 min each. Commercial reference pulse sensors were used to estimate the performance of the proposed device. An electrocardiogram, ECG (Polar N2965, Polar, FIN), which was not influenced by motion, was used as the reference pulse device, and an oximeter (MP-111, MEK, KOR) that could not reduce the motion artifacts was used for comparison. For the typing task, each subject typed sample texts from typing software with the aim of typing 400 characters per minute (cpm), as shown in Fig. 4(a). For the writing task, each subject had to write the same sample texts used in the typing task on paper. The tapping task was performed to the rhythm of pop music, and the gesturing task involved the free use of hand movements during a conversation. The walking task was performed on a treadmill (REDON-RX9200, Tobeone, KOR) at 4 km/h. The running task, shown in Fig. 4(b), was performed on the same treadmill at 8 km/h.

Additional tests were performed to obtain continuously changing heart rates. The subjects were tested on the treadmill for ten minutes, and the speed was gradually increased (4, 6, 8, 10, 4 km/h) and then sharply decreased to rest. By gradually increasing the running speed, the heart rate became faster than during a constant speed test. In this test, only the heart rate determined by the ECG was compared to that of the reconstructed device to verify its performance.

3. Results and discussion

3.1. Computational time of algorithms

Algorithms with short computation times are required for wearable devices due to the limited resources of an embedded system. The computation time of the LMS adaptive filter is compared with those of the RLS adaptive filter [11], PCA [2], ICA [4], and Lagguerre [9] in Table 1 to verify the performance of the designed algorithm. Each of the algorithms was designed to have less than 5% error. The result presents that the LMS adaptive filter has the shortest computing time among the algorithms tested.

3.2. Motion artifacts in PPG signals

To understand the motion artifacts, the distorted PPG signal, the two-directional accelerations, and the reference signal (ECG) of a single subject were analyzed. The frequency amplitude in the

Table 1
Computing time of the motion artifact reduction algorithms; each of the algorithms was simulated five times on the same computer using Matlab.

Algorithm	Adaptive Filter (LMS)	Adaptive Filter (RLS)	PCA	ICA	Lagguerre
Computing time (ms)	6.86 ± 0.12	17.98 ± 0.48	8.46 ± 1.53	51.96 ± 1.24	8.24 ± 0.18

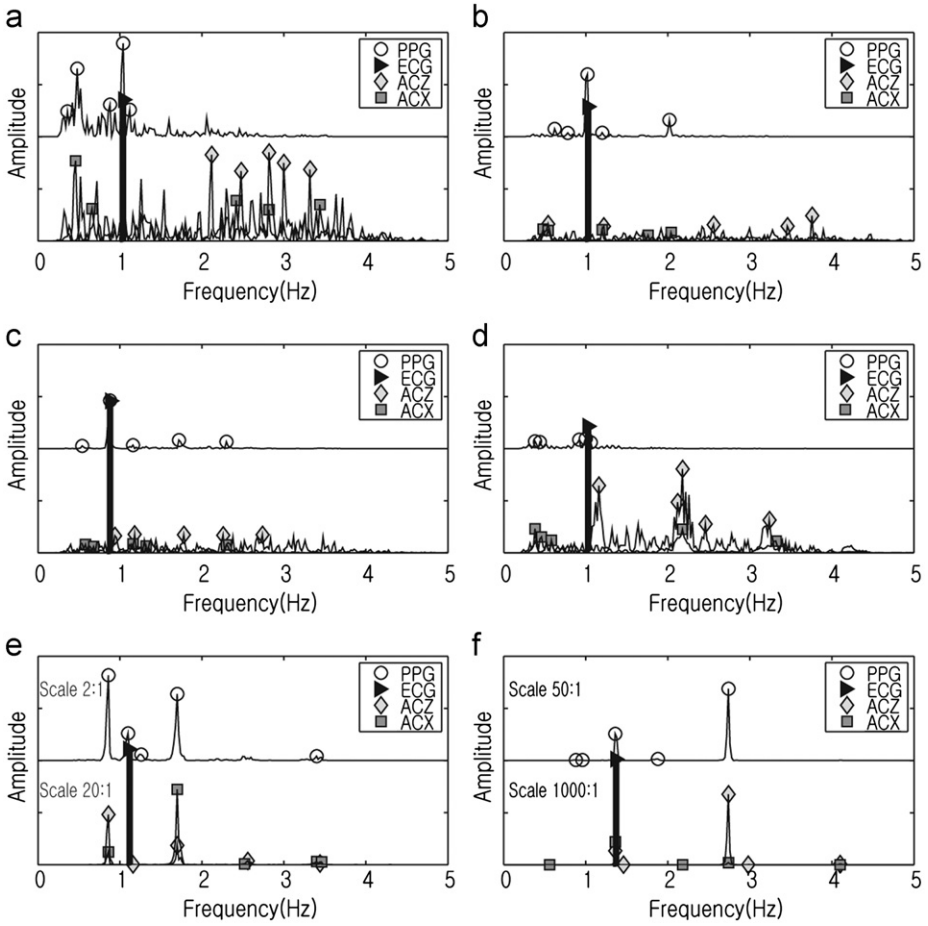

Fig. 5. Frequency properties for each motion: (a) typing, (b) writing, (c) tapping, (d) gesturing, (e) walking, and (f) running. ECG signal (►), PPG signal (○), longitudinal acceleration (ACX: ◇), and radial acceleration (ACZ: □).

frequency domain was analyzed by fast Fourier transform (FFT) while the subjects performed each of the six motions (typing, writing, tapping, and gesturing for one minute and walking and running for 5 min) with a Hanning window. Fig. 5 shows the frequency responses of the PPG signal and the accelerations in the top and bottom portions of the plots, respectively. The largest five peaks of each signal are expressed by symbols on the graphs, as is the main heart rate frequency from the reference (ECG). In the static condition, the PPG signal has only one dominant frequency component that is close to that of the ECG, and the longitudinal acceleration (ACX) and radial acceleration (ACZ) do not have any dominant frequency components. During the various motions, however, the signals are distorted and different frequency components are created; the largest PPG peak frequency is different from that of the ECG, and other PPG peaks are created. It can be seen that some of the PPG peaks overlap those of the accelerometer, and a component of the pulse frequency remains as seen by comparison with the ECG peak.

The typing test results are shown in Fig. 5(a). The accelerations illustrate that typing is a fast-changing motion in a high-frequency range and a non-periodic motion with widely distributed components. The ACX and a greater part of the ACZ are of higher frequency than the ECG, and two peaks of the ACZ are in the frequency range of the PPG signal. The PPG signal is clearly distorted, and the difference between the first and the second largest peaks of PPG signal is small. Although the largest component of the PPG signal is identical to the ECG, the fact that the second largest component of the PPG overlaps acceleration peaks indicates that the PPG is clearly affected by typing motions. For the writing task involving small hand and finger motions, the accelerations are small and widely distributed over the frequency range, as shown in Fig. 5(b). The largest peak of the PPG signal is much larger than the others and precisely overlaps that of the ECG, indicating that the PPG signal is scarcely affected by this motion. The results of the tapping task shown in Fig. 5(c) are similar to those of the writing task, though the accelerations are more crowded at low frequencies. The amplitudes of the accelerations are so small that there is almost no distortion.

The gesturing task, which involves large and random hand motions, produced a fast and wide range of accelerations as shown in Fig. 5(d). Most peaks of the ACZ and the ACX are much larger than the ECG peak. The frequency components of the PPG signal are arranged in two groups. The 1-Hz group consists of pulses, and the 0.5-Hz group consists of signals distorted by the overlapped accelerations. The two groups have similar amplitudes, indicating that the motions affect the PPG signal. Fig. 5(e) shows the results for the motion of walking. Because the amplitude of the accelerations is much larger than the aforementioned motions, the scale is changed to 20:1. The ECG is slightly greater than 1 Hz. However, the first and the second peaks of the PPG signal do not match the ECG peak, and both overlap with accelerations, indicating that the artifacts are much larger than the real pulse component. The results for the running task, which involve fast and periodic motions, are similar to those of the walking task, as shown in Fig. 5(f). Not only are the peaks of the acceleration much larger than the peaks of other motion tests, but the peaks of the PPG signal that overlap the acceleration peaks are also amplified. The peaks of the PPG signal are considered to be the effect of the artifacts.

The artifact analysis suggests that body motions directly distort the PPG signal, making it difficult to distinguish the pulse peaks. High magnitude acceleration motions in the range of general heart rate (0.7–2.5 Hz) affect the PPG signal. Accordingly, the frequency components of the PPG signal overlapped the components of the accelerations. The artifacts related to hand motions had a greater effect due to their large accelerations near the frequency of the PPG signal.

The motion artifacts are affected by tissue deformations and instantaneous local blood flow changes in the finger. Friction between the base of the finger and the surface of the sensor cause tissue shear deformation during the motion. This deformation changes the measurement site from the initial site; therefore, the sensor measures corrupted pulse waveforms at the changed site. Motion instantly changes the amount of blood that passes along digital arteries due to the inertia force of the blood. Therefore, the corrupted blood flow may be measured at the changed measurement site inside the finger. It is not easy to reduce the blood flow distortion because it occurs in the body, but the tissue deformation can be reduced. Minimization of the sensor weight can reduce the friction force between the sensor and the skin, and a sensor design that fits the finger tightly can reduce the deformation displacements. Additionally, finding a static measurement site that does not deform during motion is also important.

3.3. Motion artifact reduction

The six daily life motions were tested with the reconstructed device, the oximeter, and the ECG (reference) to analyze the performance of the motion artifacts reduction algorithm. Fig. 6 shows a case involving a dynamic condition in which the task of analyzing the true heart rate from the raw PPG is complicated. However, after the proposed algorithm was applied, the morphology of the PPG signal improved, making the pulses easier to read. The estimated heart rate also changed from 120 bpm to 76 bpm, comparing favorably to the reference value of 74 bpm. These results indicate that the algorithm reduced the artifacts dramatically.

The heart rates determined during the motion tests from the reconstructed PPG and by oximetry are plotted versus the ECG reference heart rate in Fig. 7. The center dashed–dotted line indicates the reference data and side lines represent the 5% error lines. The PPG data are mostly with the 5% error lines, but half of the oximetry data are over the error lines. In the static condition, all the devices measured a heart rate of 54 bpm. For the walking test, the heart rate determined from the PPG decreased from 115 bpm to 73 bpm upon reconstruction, which is less than 5% less than the reference heart rate of 76 bpm. For the running task, the heart rate determined from the PPG increased from 57 bpm to 108 bpm upon reconstruction, matching well with the reference heart rate of 107 bpm. The other tasks yielded similar results. Although the PPG data without the algorithm had a high rate of error, the reconstructed device reduced the error rate to less than 5%.

The reconstructed PPG and the ECG for eleven subjects walking and running on a treadmill, where the most significantly signal corruption is observed, are shown in Fig. 8(a). A wide range of heart rates, 60∼160 bpm, was obtained as the exercise intensity increased progressively. The results show errors of

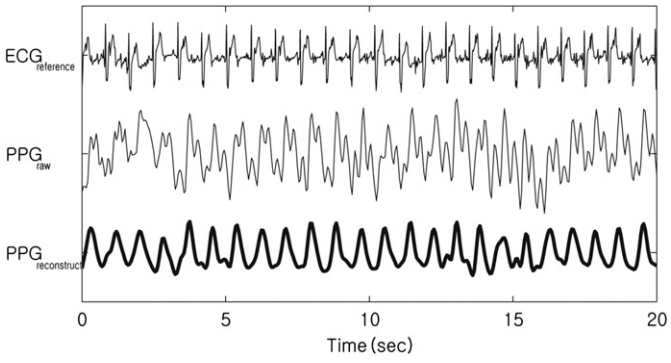

Fig. 6. Raw PPG, reconstructed PPG, and ECG signals.

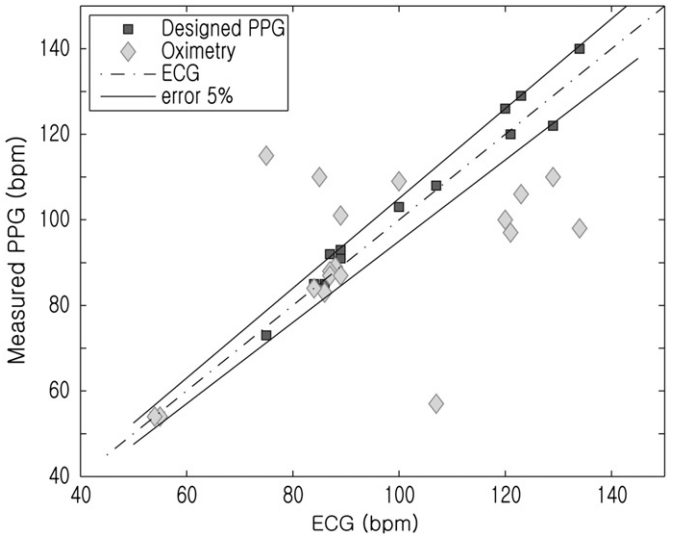

Fig. 7. Heart rates determined from reconstructed PPG and from the oximeter plotted versus the ECG reference heart rate.

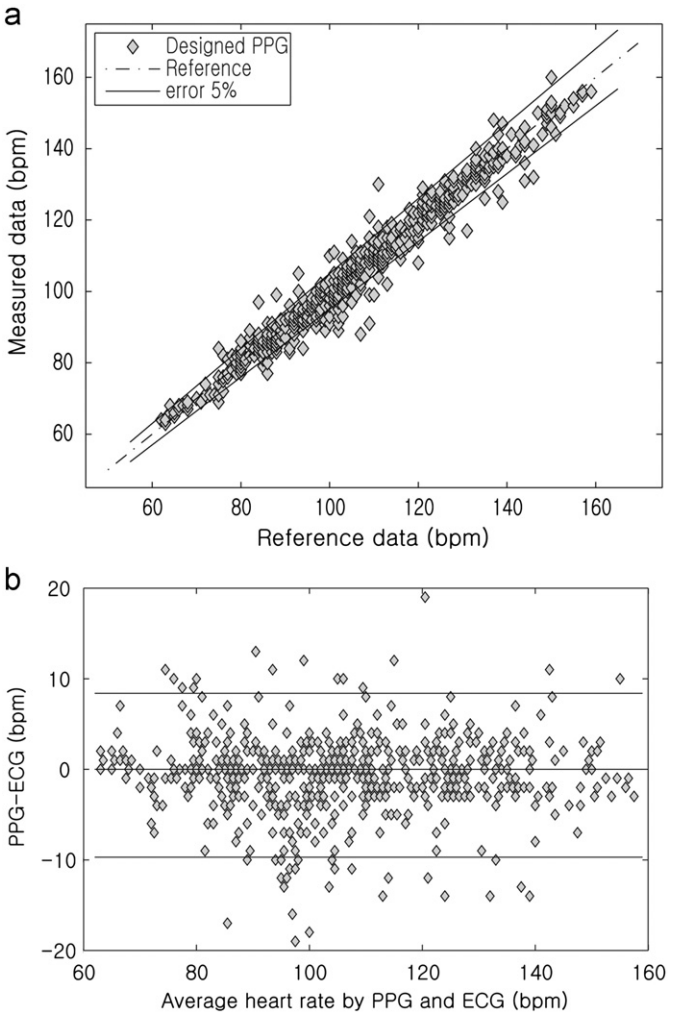

Fig. 8. Artifact reduction of PPG during walking and running; (a) error rate analysis (b) Bland Altman plot.

$2.55 \pm 2.70\%$ with most of the data between the 5% error lines. Although in a few cases, less than 10% of data, the data exceeded the error lines, the errors were not clustered together. This result indicates that the proposed algorithm is stable and that it can detect the real heart rate from the correct signal. The data were also compared in a Bland–Altman plot [24], shown in Fig. 8(b), that analyzed the agreement between the heart rates determined by the PPG and the ECG by comparing the plot of their differences (errors) versus their average with the mean error and standard deviation (SD). The PPG had a mean error of -0.6 bpm, and most of errors were between -9.7 and 8.4 bpm, which is in 95% agreement (mean $\pm$ 1.96 SD). Because most of the errors within 95% reliability are smaller than 10 bpm and because there is no error inclination due to heart rates, the reconstructed PPG device and algorithm are determined to perform acceptably.

Despite the satisfactory performance of the algorithms, there are two difficulties: poor performance of the algorithm during high speed running and individual variations. Running at speeds higher than 8 km/h produces instant impacts to whole body as the feet come into contact with the ground. The impacts cause severe local blood flow corruption and tissue deformations. The slope of the relation between speed and impact increases more rapidly in running [25] than in walking [26]. This algorithm is focused on the daily life motions, so the performance of the algorithm could be lower in high speed running. The second difficulty is individual variations in the physical properties of the skin tissue and blood pressure. The AC components of the reflected light decrease as the pathway length increases, i.e., a small pulse is obtained for subjects with thick skin tissues. Moreover, the magnitude of the blood pressure also affects the signal amplitude which differs five times individually; low blood pressure produces small pulse fluctuations. Therefore, automatic individual settings are necessary to amplify the small signal.

4. Conclusion

The artifacts in the PPG signal during the daily life motions were analyzed and reduced using a LMS-based active noise cancellation method that was applicable to the wearable devices due to the short computation time. By comparing the PPG signal with the reference pulse and the motion accelerations in the frequency domain, the artifacts were determined to arise from periodic motions in the range of the pulse frequency. Considering the directions of the blood flow on the finger, a two-dimensional LMS adaptive algorithm was applied that corrected the pulse waveform in the PPG signal by removing the motion information in the range of the pulse frequency with less than 5% heart rate error. The result of this study could be applied as a terminal in a mobile healthcare system, enabling continuous health monitoring without disturbing daily life.

5. Summary

Photoplethysmography (PPG) is regarded as a practical tool for noninvasive monitoring devices that detect heart rate, blood oxygen saturation, and respiration. One of the problems in applying PPG technology to portable devices is the signal distortion of PPG due to motion. To solve this issue, the correlation between six representative daily motions and patterns of the artifact were analyzed, and an artifact reduction algorithm was designed using the motion data. Because of the short operating time and the small number of important variables of the portable device, a LMS adaptive filter was employed and compared with other noise reduction algorithms. For validation purposes, a real-time motion artifact reduction experiment was performed using a reconstructed wearable device during the motions. The results indicate that the motion artifacts of wearable photoplethysmography devices can be

effectively reduced using the proposed method and that such devices can potentially be used in daily life with any kind of motion. This study is relevant to biomedical engineers interested in using portable health monitoring devices.

Conflict of interest statement

None Declared

Acknowledgment

This research was supported by the Happy tech. program through the National Research Foundation of Korea (NRF) funded by the Ministry of Education, Science and Technology (No. 2011-0020934).

References

[1] J. Allen, Photoplethysmography and its application in clinical physiological measurement, Physiol. Meas. 28 (2007) R1–39.
[2] R.H. Enriquez, M.S. Castellanos, J.F. Rodriguez, J.L.H. Caceres, Analysis of the photoplethysmographic signal by means of the decomposition in principal components, Physiol. Meas. 23 (2002) N17–29.
[3] Y. Yan, C.C.Y. Poon, Y. Zhang, Reduction of motion artifact in pulse oximetry by smoothed pseudo Wigner–Ville distribution, J. Neuroeng. Rehabil. 2 (2005) 3.
[4] B.S. Kim, S.K. Yoo, Motion artifact reduction in photoplethysmography using independent component analysis, IEEE Trans. Biomed. Eng. 53 (2006) 566–568.
[5] Z. Kun, J. Teng, D. Xiuzhen, Z. Wen, Extracting motional information from the photoplethysmography using reconstruction of the wavelet transforms modulus maxima, Conf. Proc. Int. Conf. Bioinform. Biomed. Eng. (2008) 1395–1398.
[6] S. Kim, E.J. Hwang, D.W. Kim, Reduction of movement artifacts in photoplethysmograph using SFLC (scaled Fourier linear combiner), IFMBE Proc. 15 (2007) 427–430.
[7] H. Shin, C. Lee, M. Lee, Adaptive threshold method for the peak detection of photoplethydmographic waveform, Comput. Biol. Med. 39 (2009) 1145–1152.
[8] P.T. Gibbs, L.B. Wood, H.H. Asada, Active motion artifact cancellation for wearable health monitoring sensors using collocated MEMS accelerometers, Proc. SPIE (2005) 811–819.
[9] H.H. Asada, H.H. Jiang, P. Gibbs, Active noise cancellation using MEMS accelerometers for motion-tolerant wearable bio-sensors, Conf. Proc. IEEE Eng. Med. Biol. Soc. (2004) 2157–2160.
[10] K.W. Chan, Y.T. Zhang, Adaptive reduction of motion artifact from photoplethysmographic recordings using a variable step-size LMS filter, Conf. Proc. IEEE Sens. 2 (2002) 1343–1346.
[11] A.R. Relente, L.G. Sison, Characterization and adaptive filtering of motion artifacts in pulse oximetry using accelerometers, IEEE Trans. Biomed. Eng. 48 (2001) 452–461.
[12] E. Zahedi, G.K. Beng, Applicability of adaptive noise cancellation to fetal heart rate detection using photoplethysmography, Comput. Biol. Med. 38 (2008) 31–41.
[13] P. Renevey, R. Vetter, J. Krauss, P. Celka, Y. Depeursinge, Wrist-located pulse detection using IR signals, activity and nonlinear artifact cancellation, Conf. Proc. IEEE Eng. Med. Biol. Soc. 3 (2001) 3030–3033.
[14] J.Y.A. Foo, S.J. Wilson, A computational system to optimise noise rejection in photoplethysmography signals during motion or poor perfusion states, Med. Biol. Eng. Comput. 44 (2006) 140–145.
[15] E. Kunesch, F. Binkofski, H.J. Freund, Invariant temporal characteristics of manipulative hand movements, Exp. Brain Res. 78 (1989) 539–546.
[16] K. Watanabe, T. Watanabe, H. Watanabe, H. Ando, T. Ishikawa, K. Kobayashi, Noninvasive measurement of heartbeat, respiration, snoring and body movements of a subject in bed via a pneumatic method, IEEE Trans. Biomed. Eng. 52 (2005) 2100–2107.
[17] Y. Xiong, F. Quek, Hand motion gesture frequency properties and multimodal discourse analysis, Int. J. Comput. Vision 69 (2006) 353–371.
[18] R.R. Anderson, J.A. Parrish, The optics of human skin, J. Invest. Dermatol. 77 (1981) 13–19.
[19] M. Nitzan, A. Babchenko, D. Shemesh, J. Alberton, Influence of thoracic sympathectomy on cardiac induced oscillations in tissue blood volume, Med. Biol. Eng. Comput. 39 (2001) 579–583.
[20] U. Schultz-Ehrenburg, V. Blazek, Value of quantitative photoplethysmography for functional vascular diagnostics, Skin Pharmacol. Physiol. 14 (2000) 316–323.
[21] B. Widrow, J.R. Glover Jr, J.M. McCool, J. Kaunitz, C.S. Williams, R.H. Hearn, J.R. Zeidler, E. Dong Jr, R.C. Goodlin, Adaptive noise cancelling: principles and applications, Proc. IEEE 63 (1975) 1692–1716.
[22] S. Haykin, B. Widrow, Least-Mean-Square Adaptive Filters, Wiley-Interscience, New York, 2003, pp. 1–34.
[23] H. Han, M.J. Kim, J. Kim, Development of real-time motion artifact reduction algorithm for a wearable photoplethysmography, Conf. Proc. IEEE Eng. Med. Biol. Soc. (2007) 1538–1541.
[24] J.M. Bland, D.G. Altman, Measuring agreement in method comparison studies, Stat. Methods Med. Res. 8 (1999) 135–160.
[25] T.S. Keller, A.M. Weisberger, J.L. Ray, S.S. Hasan, R.G. Shiavi, D.M. Spengler, Relationship between vertical ground reaction force and speed during walking, slow jogging, and running, Clin. Biomech. (Bristol, Avon) 11 (1996) 253–259.
[26] P. Luhtanen, P.V. Komi, Force-, power-, and elasticity-velocity relationships in walking, running, and jumping, Eur. J. Appl. Physiol. Occup. Physiol. 44 (1980) 279–289.

Hyonyoung Han received the B.S. degree in mechanicalengineering in 2005 from KAIST, Deajeon, Korea, and the M.S. degree in mechanical engineering in 2007 from KAIST, Daejeon, Korea, where he is currently working toward the Ph.D. degree in mechanical engineering. His current research interests include health monitoring, biosignal, and bioinstrumentation.

Jung Kim (M'05) received the Ph.D. degree from the Department of Mechanical Engineering, Massachusetts Institute of Technology, Cambridge. He is an Associate Professor in the Department of mechanical engineering, KAIST, Daejeon, Korea. His current research interests include haptic interactions in virtual environments, soft-tissue modeling, medical robotics, medical simulation, and biological cellular manipulation.